ADVANCED MATERIALS

High-Performance Organic Single-Crystal Transistors and Digital Inverters of an Anthracene Derivative

By *Lang Jiang, Wenping Hu,* Zhongming Wei, Wei Xu,* and *Hong Meng**

Organic single-crystalline micro- and nanostructures synthesized from π-conjugated molecules have attracted particular interest as building blocks for optoelectronic devices such as field-effect transistors,[1–3] photoswitches,[4] and complementary inverters.[5] Compared to organic thin films, single crystals can show intrinsic charge-transport properties and high mobility,[3,6–8] owing to the absence of grain boundaries and the minimized concentration of charge traps. They provide the opportunity to elucidate the relationship between microscopic molecular packing and macroscopic charge transport for the design of new semiconductor materials with high performance.

Complementary inverters are basic building blocks of complex integrated circuits. Organic inverters[5,9] of thin films have been successfully demonstrated, but few inverters consisting of organic single crystals have been proposed, regardless of the great merits of organic single crystals for high-performance circuits. Moreover, it is always desired that both p- and n-type semiconductors have similar mobilities for the construction of high-speed complementary inverters. This has remained a great challenge owing to the lack of high-mobility, air-stable n-type organic semiconductors. Here, we introduce a kind of high-performance digital inverter involving the integration of p-type organic single-crystal transistors only. The organic semiconductor adopted for this study is an anthracene derivative, di(phenylvinyl) anthracene (DPV-Ant, Fig. 1a).[10] The reasons for selecting it as the candidate are[10] its high yield by facile synthesis, its high performance in thin-film transistors, and its high stability in air.

Single crystals of DPV-Ant were grown by a physical vapor transport technique in a two-zone horizontal-tube furnace.[11] A quartz boat with DPV-Ant powder was placed in the high-temperature zone (220 °C) with high-purity argon used as the carrier gas (100 mL min^{-1}). Regular hexagonal disks of micro- or nanometer size were synthesized on the octadecyltrichlorosilane (OTS)-modified SiO_2 substrate placed in the 80–120 °C temperature zone. Figure 1b shows a low-magnification scanning electron microscopy (SEM) image of a large number of single-crystalline disks. The typical size of the crystalline disks ranges from several micrometers to tens of micrometers, with the thickness varying from 18 nm to several hundred nanometers (see Supporting Information 1). The crystal surface of the individual disks was very flat, as shown in Figure 1c, which was important in order to guarantee intimate contact between the crystal and gate insulator during transistor fabrication. In addition, the crystal disks could be bent easily, as shown in Figure 1d, indicating their excellent flexibility. When the disk crystals were bent by mechanical probes, they did not fracture even when they were bent more than 180° (see Supporting Information 2). The bent disks even recovered their original morphology as soon as the force from the probes was removed. This excellent flexibility demonstrates the potential of the organic single crystals for applications in flexible devices.

Single-crystal X-ray diffraction (XRD) patterns of large crystals demonstrated that the crystals of DPV-Ant belong to the $P\,2_12_12_1$ space group with $a = 5.888(2)$ Å, $b = 7.344(3)$ Å, and $c = 44.928(18)$ Å (for a cif file of the crystal see Supporting Information 3). From the crystal-structure analysis, molecules of DPV-Ant were demonstrated to be packed in a herringbone geometry in the crystals (Fig. 2a,b), which is similar to the packing of pentacene molecules in crystals.[12]

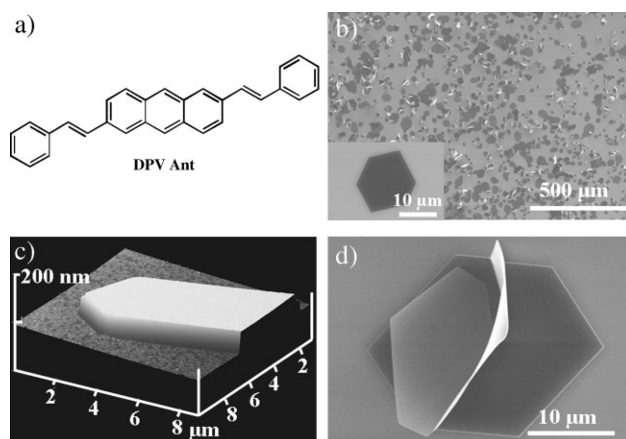

Figure 1. a) Molecular structure of DPV-Ant. b) Large-area SEM image of DPV-Ant single crystals. Inset: Individual single-crystalline disk. c) AFM image of a part of an individual hexagonal single crystal. The thickness of the crystal was around 86 nm. d) SEM image of a bent single-crystal disk.

[*] Prof. W. P. Hu, L. Jiang, Z. M. Wei, Prof. W. Xu
Beijing National Laboratory for Molecular Sciences
Key Laboratory of Organic Solids
Institute of Chemistry
Chinese Academy of Sciences
Beijing 100080 (P.R. China)
E-mail: huwp@iccas.ac.cn

Dr. H. Meng
Central Research and Development
Experimental Station
E. I. DuPont Company
Wilmington, DE 19880 (USA)
E-mail: hong.meng@usa.dupont.com

L. Jiang, and Z. Wei
Graduate University of the Chinese Academy of Sciences
Beijing 100039 (P.R. China)

DOI: 10.1002/adma.200900503

© 2009 WILEY-VCH Verlag GmbH & Co. KGaA, Weinheim

WILEY InterScience® DISCOVER SOMETHING GREAT

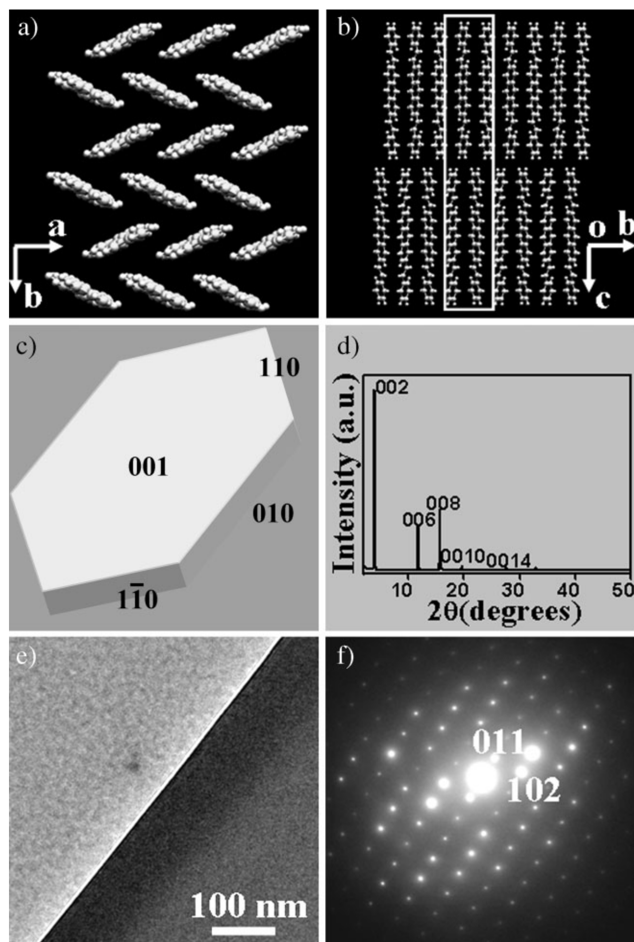

Figure 2. Crystal packing of DPV-Ant molecule with views of a) the *ab*-plane and b) the *bc*-plane. c) Schematic diagram of the single crystals with indexed growth surface. d) Powder XRD pattern of DPV-Ant crystals. e) TEM image of the DPV-Ant single crystal and f) its corresponding SAED pattern.

The shapes of the crystal disks were so regular (for example, Fig. 1d) that the crystal facets could be indexed directly according to the law of constancy of interfacial angles by inspection of their appearance under SEM. An indexed schematic diagram of a DPV-Ant single crystal with all habit faces is shown in Figure 2c. This diagram, as well as the SEM and atomic force microscopy (AFM) images, indicates that the (001) plane of the crystal is parallel to the surface of the substrate. A powder XRD pattern of the disks is shown in Figure 2d. The baseline is very straight and the diffraction peaks are very sharp, indicating the high quality of the DPV-Ant single crystals. All the peaks in this pattern were well indexed to the orthorhombic phase according to the XRD results of DPV-Ant single crystals. The (00*l*) lattice plane in the DPV-Ant disks was parallel to the substrate, that is, DPV-Ant molecules could grow in a step-like, layer-by-layer growth mode, which agrees well with the results according to the law of constancy of interfacial angles. A step-like structure was clearly observed on the surface of single crystals grown in the low-temperature zone, and the average height of steps was about 2.35 nm (see Supporting Information 4), which approached half of the (001) *d*-spacing value of the DPV-Ant single crystal (Fig. 2b), indicating a layer-by-layer growth mechanism of the single crystal. A typical transmission electron microscopy (TEM) image of the disk is given in Figure 2e, and its corresponding selected-area electron diffraction (SAED) pattern is shown in Figure 2f. The SAED pattern could be indexed based on an orthorhombic cell with lattice parameters $a = 5.888(2)$ Å, $b = 7.344(3)$ Å, and $c = 44.928(18)$ Å, consistent with the above-mentioned single-crystal and powder XRD results. No change of the SAED pattern was observed at different parts of the same disk, indicating that the whole disk was a single crystal.

The fabrication of transistors based on such small single crystals encountered some technological challenges, because organic crystals are bonded by relatively weak van der Waals forces, which can be easily damaged by conventional micro-fabrication techniques such as electron-beam deposition and focused-ion-beam deposition. In order to avoid these problems, the "organic ribbon mask" method[13] was used to fabricate in situ top-contact transistors based on the small organic single crystals on Si/SiO_2 (500 nm) substrates (low-resistance Si as the back gate). Typical SEM images of the device are shown in Figure 3a–d, where the channel length ranging from 1 to 20 μm is tuned by the size of the "ribbon mask".[13] All devices exhibited p-type transistor behavior and the carrier transport was along the *a*-axis. Interestingly, we were able to examine the carrier transport along the *b*-axis (Fig. 3e) in the disk crystals, and even the mobility anisotropy of an individual crystal, using crossed ribbons as a shadow mask (Fig. 3f).

Representative output and transfer characteristics of the devices based on an individual DPV-Ant single-crystal disk are shown in Figure 4a and b. The devices exhibited very weak hysteresis, as shown in the transfer curves, indicating the

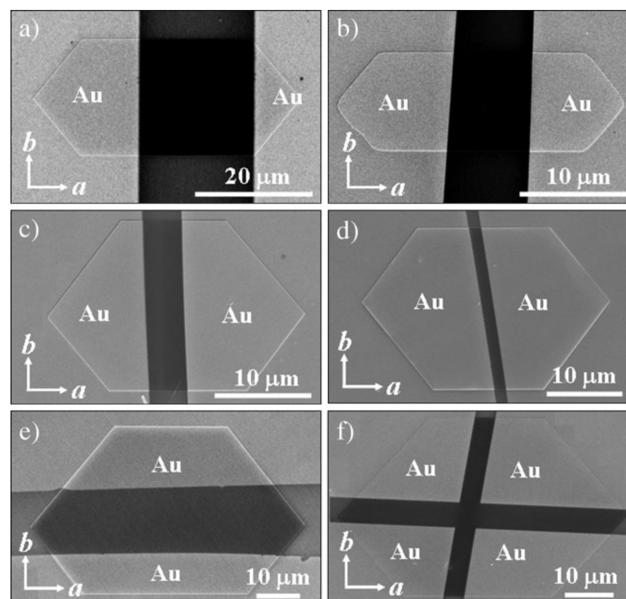

Figure 3. a–f) SEM images of DPV-Ant transistors based on individual single-crystal disks with channel lengths varying from 1 to 20 μm and a–d) carrier transport along *a*-axis, e) with carrier transport along *b*-axis, and f) with channels parallel to the crystallographic axes, that is, with carrier transport along the *a*- and *b*-axes.

WILEY InterScience® DISCOVER SOMETHING GREAT
© 2009 WILEY-VCH Verlag GmbH & Co. KGaA, Weinheim

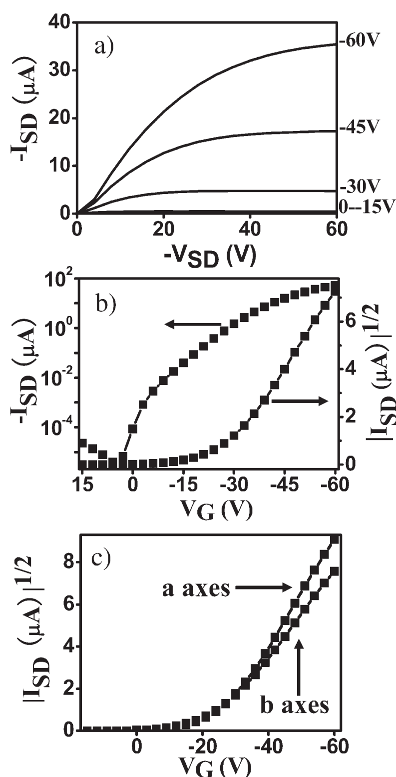

Figure 4. Typical a) output and b) transfer characteristics of DPV-Ant transistors based on individual single-crystal disks. c) Transfer characteristics along the *a*-and *b*-axes of DPV-Ant transistors based on individual single-crystal disks.

reduction of charge-trapping effects, that is, the quality of the small interface between the in situ patterned single-crystalline disk and the OTS-modified SiO_2 insulator is high. According to the transfer characteristics, the mobility μ, threshold voltage, and on/off ratio of the devices were calculated to be 1.6–4.3 $cm^2\ V^{-1}\ s^{-1}$, −14 to −33 V, and $\sim 10^5$–10^7, respectively. Over 90% of the 30 devices exhibited mobility above 2.0 $cm^2\ V^{-1}\ s^{-1}$. The highest mobility of DPV-Ant single crystals was 4.3 $cm^2\ V^{-1}\ s^{-1}$, along the *a*-axis with on/off ratio of 5.0×10^6. The mobility along the *b*-axis was lower than the one along the *a*-axis. The highest mobility along the *b*-axis was 2.2 $cm^2\ V^{-1}\ s^{-1}$. The mobility-anisotropy ratio μ_a/μ_b was 1.5–1.95, calculated from ten transistors as in Figure 3f with different channels along the *a*- and *b*-axes based on an individual microcrystal. Representative results are shown in Figure 4c. As shown in Figure 2a, a more dense molecular packing was observed along the *a*-axis than along the *b*-axis, indicating stronger intermolecule interactions along the *a*-axis. It is believed that stronger intermolecular interactions could induce stronger overlap between the π-orbitals of adjacent molecules, and result in higher mobility. Obviously, the mobility anisotropy coincides with the fact that the stronger-intermolecular-interaction direction, along the *a*-axis, shows higher mobility, and the weaker-intermolecular-interaction direction, along the *b*-axis, exhibits lower mobility.

From the output characteristics of the transistors shown in Figure 4a, it appeared that the drain current was obviously limited at low applied-voltage V_{SD} by the contact resistance. As we know, the contact resistance of transistors results from unfavorable matching of the Fermi level of the metal contacts with the highest occupied molecular orbital (HOMO) level of the semiconductor, or high-resistance paths from the metal contacts on the surface of the crystals to the carrier channel near the bottom surface of the crystals. Transistors based on single crystals of different thickness (see Supporting Information 1) showed that the drain current was severely limited by the contact resistance, as the thickness of the single crystal increased from 18 nm to 348 nm. Therefore, the contact resistance of the DPV-Ant single-crystal transistors is mostly determined by the resistance from the metal contacts on the surface of the crystals to the carrier channel near the bottom surface of the crystals. It was also found that the transistor performance decreased with increasing crystal thickness: when the thickness of the single crystal was 348 nm, the mobility was only about 0.4 $cm^2\ V^{-1}\ s^{-1}$. Hence, it is important to select thin-enough single-crystal disks to eliminate the effects of the contact resistance. Interestingly, it was noticed that the color of the single crystals depends on their thickness. For example, the crystal was pea green when its thickness was ~18 nm, shifting to dark blue at ~54 nm and finally yellow at ~348 nm (see Supporting Information 1). Therefore, this provides us a feasible way to estimate and select crystals with different thicknesses.

Digital inverters consisting of two top-contact p-type single-crystal transistors were fabricated. The circuit diagram of the inverter is shown in Figure 5a, and the corresponding device schematic in Figure 5b. For fabrication of the inverter, gate electrodes were first produced on the SiO_2/Si substrates by sputtering a 5 nm Ti adhesion layer followed by 40 nm Au using a shadow mask. Then, about 600 nm poly(methylmethacrylate) (PMMA) was spin-coated on the gate electrodes as a dielectric. An individual DPV-Ant single-crystalline disk was picked up from the other substrates by a mechanical probe and placed on the gate insulator. Finally, thin Au layers (about 100 nm) were glued onto the disk as source and drain electrodes as well as interconnection.[14] Figure 5c shows the transfer characteristics of the inverter. The inverter was operated under several V_{DD} conditions:

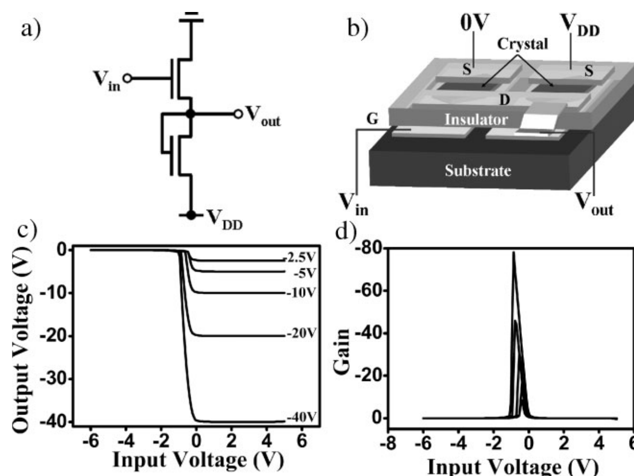

Figure 5. a) Circuit diagram of the inverter. b) Device schematic of the inverter. c) Transfer characteristics of the inverter operated at supply voltages between −2.5 V and −40 V. d) Signal gain of the inverter.

© 2009 WILEY-VCH Verlag GmbH & Co. KGaA, Weinheim
WILEY InterScience® DISCOVER SOMETHING GREAT

$V_{DD} = -40$, -20, -10, -5, and -2.5 V, and it is interesting that our inverter operated well over a wide voltage range, even at a low V_{DD} of -2.5 V. The inverter showed ideal transfer curves with excellent logic-level conservation. The output-voltage swings of the inverters were very close to the value of the corresponding applied voltage V_{DD}, that is, the output voltage started from values very close to the applied voltage V_{DD} and then dramatically dropped to very low values. Here, the output voltage swing was defined as the difference between the maximum and minimum values of the output voltage. As shown in Figure 4d, the voltage gains increased with higher V_{DD}, the corresponding values being 8.5, 17.3, 30.8, 45.8, and 78.6 for $V_{DD} = -2.5$, -5, -10, -20, and -40 V, respectively; the maximum gain was ~80.

In summary, micrometer- and nanometer-sized single-crystalline disks of DPV-Ant were produced by the physical vapor transport technique. Single-crystalline transistors with high performance were fabricated by the organic ribbon mask method. The mobility of the transistors based on an individual disk approached ~4.3 $cm^2\ V^{-1}\ s^{-1}$, which is one of the highest mobilities of organic transistors based on anthracene derivatives. The mobility anisotropy along different crystalline axes was also studied, and the mobility anisotropy ratio μ_a/μ_b was around 1.5–1.95; the stronger the intermolecular interaction, the higher the mobility. Combining two high-performance p-type single-crystalline transistors, a digital inverter with high gain was fabricated.

Experimental

Substrates used in the present study were successively cleaned with pure water, hot acetone, pure ethanol, piranha solution (H_2SO_4/H_2O_2 7:3), pure water, hot ammonia/hydrogen peroxide solution (ammonia / hydrogen peroxide / water 1:1:5), pure water, and pure ethanol. Treatment of the Si/SiO_2 wafer with OTS was carried out by vapor deposition. The clean wafers were dried under vacuum at 100 °C for 0.5 h in order to eliminate the influence of moisture. After the wafers had cooled to room temperature, one drop of OTS was placed on them. Subsequently, this system was heated to 120 °C and maintained at this temperature for 2 h under vacuum.

Single-crystal disks of DPV-Ant were synthesized by the physical vapor transport technique through a two-zone horizontal-tube furnace evacuated by a mechanical pump. A quartz boat containing DPV-Ant powder was placed in the high-temperature zone (220 °C). High-purity argon was used as the carrier gas (100 sccm). Single-crystal disks of DPV-Ant were obtained on substrates in the low-temperature zone (80–120 °C). For the fabrication of transistors, DPV-Ant crystals were first grown on Si/SiO_2/OTS substrates by physical vapor transport (here the thickness of the SiO_2 dielectric was ~500 nm). Then drain and source electrodes (~40 nm) were deposited on the single crystals by thermal evaporation with an organic ribbon as a shadow mask [13]. Finally, the organic ribbon was removed to obtain a gap between the source and drain electrodes. For the fabrication of inverters, discrete gate electrodes were first produced on the Si/SiO_2 substrates by sputtering a 5 nm Ti adhesion layer followed by 40 nm Au using a shadow mask. Then ~600 nm PMMA was spin-coated on the gate electrodes as the dielectric. An individual DPV-Ant single crystal was picked up from the other substrates by a mechanical probe and placed on the PMMA dielectric. Finally, thin Au layers (about 100 nm) were glued onto the crystal as source and drain electrodes as well as interconnection [14]. Current–voltage (*I–V*) characteristics of the transistors and transfer characteristics of the inverter were recorded using a Keithley 4200-SCS semiconductor parameter analyzer and a micromanipulator 6150 probe station in a clean and shielded box in ambient laboratory environment at room temperature. SEM images were obtained using a Hitachi S-4300 (Japan); TEM and SAED measurements were carried out using a JEOL-2010 (Japan). XRD was measured using a D/max2500 with Cu Kα source ($\lambda = 1.541$ Å).

Acknowledgements

The authors acknowledge financial support from the National Natural Science Foundation of China (20721061, 20872146, and 50725311), the Ministry of Science and Technology of China, and the Chinese Academy of Science. Supporting Information is available online from Wiley InterScience or from the authors.

Received: February 13, 2009
Revised: March 11, 2009
Published online: May 18, 2009

[1] a) M. L. Tang, A. D. Reichardt, T. Siegrist, S. C. B. Mannsfeld, Z. Bao, *Chem. Mater.* **2008**, *20*, 4669. b) T. Okamoto, M. L. Senatore, M. Ling, A. B. Mallik, M. Tang, Z. Bao, *Adv. Mater.* **2007**, *19*, 3381. c) H. Moon, R. Zeis, E. Borkent, C. Besnard, A. J. Lovinger, T. Siegrist, C. Kloc, Z. Bao, *J. Am. Chem. Soc.* **2004**, *126*, 15322. d) H. E. Katz, Z. Bao, S. L. Gilat, *Acc. Chem. Res.* **2001**, *34*, 359. e) H. Meng, F. P. Sun, M. B. Goldfinger, F. Gao, D. J. Londono, W. J. Marshal, G. S. Blackman, K. D. Dobbs, D. E. Keys, *J. Am. Chem. Soc.* **2006**, *128*, 9304. f) H. Meng, F. P. Sun, M. B. Goldfinger, G. D. Jaycox, Z. G. Li, W. J. Marshall, G. S. Blackman, *J. Am. Chem. Soc.* **2005**, *127*, 2406. g) H. Meng, Z. Bao, A. J. Lovinger, B. Wang, A. M. Mujsce, *J. Am. Chem. Soc.* **2001**, *123*, 9214.

[2] a) A. L. Briseno, S. C. B. Mannsfeld, X. M. Lu, Y. J. Xiong, S. A. Jenekhe, Z. Bao, Y. Xia, *Nano Lett.* **2007**, *7*, 668. b) D. H. Kim, J. T. Han, Y. D. Park, Y. Jang, J. H. Cho, M. Hwang, K. Cho, *Adv. Mater.* **2006**, *18*, 719. c) S. X. Xiao, J. Y. Tang, T. Beetz, X. F. Guo, N. Tremblay, T. Siegrist, Y. M. Zhu, M. Steigerwald, C. Nuckolls, *J. Am. Chem. Soc.* **2006**, *128*, 10700. d) X. J. Zhang, G. D. Yuan, Q. S. Li, B. Wang, X. H. Zhang, R. Q. Zhang, J. C. Chang, C. Lee, S. Lee, *Chem. Mater.* **2008**, *20*, 6945. e) Q. X. Tang, L. Jiang, Y. H. Tong, H. X. Li, Y. Q. Liu, Z. H. Wang, W. P. Hu, Y. Q. Liu, D. B. Zhu, *Adv. Mater.* **2008**, *20*, 2947. f) Q. Tang, H. Li, M. He, W. Hu, C. Liu, K. Chen, C. Wang, Y. Liu, D. Zhu, *Adv. Mater.* **2006**, *18*, 65.

[3] a) H. Klauk, *Organic Electronics: Materials, Manufacturing, and Applications*, Wiley-VCH, Weinheim, Germany **2006**.[b)]E. Ahmed, A. L. Briseno, Y. Xia, S. A. Jenekhe, *J. Am. Chem. Soc.* **2008**, *130*, 1118. c) D. H. Kim, D. Y. Lee, H. S. Lee, W. H. Lee, Y. H. Kim, J. I. Han, K. Cho, *Adv. Mater.* **2007**, *19*, 678. d) H. Jiang, X. J. Yang, Z. D. Cui, Y. C. Liu, H. X. Li, W. P. Hu, Y. Q. Liu, D. B. Zhu, *Appl. Phys. Lett.* **2007**, *91*, 123505.

[4] Q. X. Tang, L. Q. Li, Y. B. Song, Y. L. Liu, H. X. Li, W. Xu, Y. Q. Liu, W. P. Hu, D. B. Zhu, *Adv. Mater.* **2007**, *19*, 2624.

[5] A. L. Briseno, S. C. B. Mannsfeld, C. Reese, J. M. Hancock, Y. J. Xiong, S. A. Jenekhe, Z. Bao, Y. Xia, *Nano Lett.* **2007**, *7*, 2847.

[6] a) I. N. Hulea, S. Russo, A. Molinari, A. F. Morpurgo, *Appl. Phys. Lett.* **2006**, *88*, 113512. b) M. F. Calhoun, C. Hsieh, V. Podzorov, *Phys. Rev. Lett.* **2007**, *98*, 096402. c) R. Zeis, T. Siegrist, C. Kloc, *Appl. Phys. Lett.* **2005**, *86*, 022103. d) V. Podzorov, V. M. Pudalov, M. E. Gershenson, *Appl. Phys. Lett.* **2003**, *82*, 1739.

[7] a) O. D. Jurchescu, S. Subramanian, R. J. Kline, S. D. Hudson, J. E. Anthony, T. N. Jackson, D. J. Gundlach, *Chem. Mater.* **2008**, *20*, 6733. b) K. Yamada, T. Okamoto, K. Kudoh, A. Wakamiya, S. Yamaguchi, J. Takeya, *Appl. Phys. Lett.* **2007**, *90*, 072102. c) Y. Xia, V. Kalihari, C. D. Frisbie, N. K. Oh, J. A. Rogers, *Appl. Phys. Lett.* **2007**, *90*, 162106. d) C. Reese, Z. Bao, *Mater. Today* **2007**, *10*, 20. e) I. N. Hulea, S. Fratini, H. Xie, C. L. Mulder, N. N. Iossad, G. Rastelli, S. Ciuchi, A. F. Morpurgo, *Nat. Mater.* **2006**, *5*, 982. f) R. W. I. de Boer, M. E. Gershenson, A. F. Morpurgo, V. Podzorov, *Phys. Status Solidi A* **2004**, *201*, 1302.

© 2009 WILEY-VCH Verlag GmbH & Co. KGaA, Weinheim

[8] a) V. C. Sundar, J. Zaumseil, V. Podzorov, E. Menard, R. L. Willett, T. Someya, M. E. Gershenson, J. A. Rogers, *Science* **2004**, *303*, 1644. b) O. D. Jurchescu, J. Baas, T. T. M. Palstra, *Appl. Phys. Lett.* **2004**, *84*, 3061. c) E. Menard, V. Podzorov, S.-H. Hur, A. Gaur, M. E. Gershenson, J. A. Rogers, *Adv. Mater.* **2004**, *16*, 2097. d) M. Mas-Torrent, M. Durkut, P. Hadley, X. Ribas, C. Rovira, *J. Am. Chem. Soc.* **2004**, *126*, 984. e) V. Podzorov, S. E. Sysoev, E. Loginova, V. M. Pudalov, M. E. Gershenson, *Appl. Phys. Lett.* **2003**, *83*, 3504.

[9] a) E. J. Meijer, D. M. de Leeuw, S. Setayesh, E. van Veenendaal, B. H. Huisman, P. W. M. Blom, J. C. Hummelen, U. Scherf, T. M. Klapwijk, *Nat. Mater.* **2003**, *2*, 678. b) M. Ling, Z. Bao, P. Erk, M. Koenemann, M. Gomez, *Appl. Phys. Lett.* **2007**, *90*, 093508. c) M. Kitamura, Y. Arakawa, *Appl. Phys. Lett.* **2007**, *91*, 053505. d) S. De Vusser, S. Steudel, K. Myny, J. Genoe, P. Heremans, *Appl. Phys. Lett.* **2006**, *88*, 162116.

[10] H. Klauk, U. Zschieschang, R. T. Weitz, H. Meng, F. Sun, G. Nunes, D. E. Keys, C. R. Fincher, Z. Xiang, *Adv. Mater.* **2007**, *19*, 3882.

[11] R. A. Laudise, C. Kloc, P. G. Simpkins, T. Siegrist, *J. Cryst. Growth* **1998**, *187*, 449.

[12] J. Cornil, J. P. Calbert, J. L. Brédas, *J. Am. Chem. Soc.* **2001**, *123*, 1250.

[13] L. Jiang, J. H. Gao, E. J. Wang, H. X. Li, Z. H. Wang, W. P. Hu, L. Jiang, *Adv. Mater.* **2008**, *20*, 2735.

[14] Q. X. Tang, Y. H. Tong, H. X. Li, Z. Y. Ji, L. Q. Li, W. P. Hu, Y. Q. Liu, D. B. Zhu, *Adv. Mater.* **2008**, *20*, 1511.

© 2009 WILEY-VCH Verlag GmbH & Co. KGaA, Weinheim
WILEY InterScience® DISCOVER SOMETHING GREAT